

# Abstract book

## 19th Kuopio Bio-MRI Workshop

Advanced MRI methods for assessment of microstructure, metabolism and function

... Supported by...



UNIVERSITY OF  
EASTERN FINLAND



Tieteellisten seuran  
valtuuskunta

charles river | every step  
of the way.



SIEMENS  
Healthineers



## Contents

### Tue, May 31th – Microstructural MRI

#### Invited speakers

Sune Jespersen.....	3
Marco Palombo.....	4
Els Fieremans.....	5

#### Short talks

Nina Hänninen .....	6
Ali Abdollahzadeh .....	7
Mohammad Khateri.....	8

#### Poster presentations

Juan Miguel Valverde.....	9
Isabel San Martín Molina .....	10
Omar Narvaez .....	11

### Wed, June 1st – Functional MRI (fMRI)

#### Invited speakers

Xin Yu.....	12
Ian Shih.....	13
Jang-Yeon Park .....	14

#### Short talks

Jaakko Paasonen .....	15
Hanne Laakso .....	16
Lenka Dvořáková.....	17

#### Poster presentations

Ekaterina Paasonen.....	18
Petteri Stenroos .....	19
Eppu Manninen.....	20

### Thu, June 2nd – Metabolic MRI and PET/MRI

#### Invited speakers

Uwe Himmelreich .....	21
Christoffer Laustsen .....	22
Andrea Capozzi .....	23

#### Short talks

Viivi Hyppönen .....	24
----------------------	----

# Modeling of gray and white matter microstructure from diffusion MRI

## Sune Jespersen

Aarhus University, Denmark  
CFIN/MindLab and Dept. of Physics and Astronomy

MRI is typically limited to providing a range of differently “weighted images” with millimeter resolution and contrast reflecting physical properties with no clear biological relevance, hampering progress in the diagnosis and treatment of neurodegenerative diseases in general. Indeed, when brain abnormalities are first noticed with MRI, the biological underpinnings are often obscure, and neurodegenerative diseases have advanced too far to be effectively treated or even managed.

But by harnessing the versatility of MRI contrast mechanisms, combined with validated biophysical modeling of its relation to tissue structure on the micrometer scale (microstructure), both enhanced sensitivity and biological specificity on the cellular scale can be achieved, effectively enabling in-vivo, MRI based, super-resolution microscopy.

In this talk, I will discuss modeling of diffusion MRI in the white and gray matter of the brain. I will present the details of the so-called Standard Model of diffusion in brain white matter, including validation studies, parameter estimation, and applications. I will then move on and discuss recent efforts of extending modeling to gray matter and give examples of their applications in ex vivo rodent, and in vivo rodent and human brains.

# Advanced mapping of tissue microstructure through MR imaging and spectroscopy

## Marco Palombo

Cardiff University, UK  
Brain Research Imaging Centre (CUBRIC)

**Abstract:** This talk presents advancements and exciting new perspectives on quantifying brain tissue structure at the cellular scale (the so-called microstructure) through diffusion-weighted MR imaging (dMRI) and spectroscopy (dMRS). I will showcase examples of how combining dMRI and dMRS measurements with computational modelling and machine learning offers unique capabilities to quantify the brain microstructure non-invasively. I will discuss potential applications to several brain diseases and future directions of research.

**Bio:** I am UKRI Future Leaders Fellow and joint Senior Lecturer (Associate Professor) at the Cardiff University Brain Imaging Research Centre (CUBRIC) - School of Psychology and the School of Computer Science and Informatics at Cardiff University. My background is in physics with a PhD in biophysics; my research focuses on developing new imaging techniques based on magnetic resonance (MR) to quantify tissue structure at the cellular scale (microstructure) non-invasively. Examples include the combined use of advanced computational modelling and machine learning to analyse diffusion-weighted MR imaging and spectroscopy data and quantify brain microstructure at histological level.

### Useful References:

Palombo et al. PNAS 2016: <https://doi.org/10.1073/pnas.1504327113>;  
Nedjati-Gilani et al. Neuroimage 2017: <https://doi.org/10.1016/j.neuroimage.2017.02.013>;  
Palombo et al. Neuroimage 2018: <https://doi.org/10.1016/j.neuroimage.2017.11.028>;  
Palombo et al. Neuroimage 2018: <https://doi.org/10.1016/j.neuroimage.2017.05.003>;  
Palombo et al. Neuroimage 2019: <https://doi.org/10.1016/j.neuroimage.2018.12.025>;  
Ligneul et al. Neuroimage 2019: <https://doi.org/10.1016/j.neuroimage.2019.02.046>;  
Callaghan et al. Neuroimage 2020: <https://doi.org/10.1016/j.neuroimage.2020.117107>;  
Jelescu et al. J Neu Meth 2020: <https://doi.org/10.1016/j.jneumeth.2020.108861>;  
Palombo et al. Neuroimage 2020: <https://doi.org/10.1016/j.neuroimage.2020.116835>;  
Hill et al. Neuroimage 2021: <https://doi.org/10.1016/j.neuroimage.2020.117425>;  
Buizza et al. Med Phys 2021: <https://doi.org/10.1002/mp.14689>;  
lanus et al. Neuroimage 2021: <https://doi.org/10.1016/j.neuroimage.2021.118424>;  
Gyori et al. Magn Reson Med 2021: <https://doi.org/10.1002/mrm.29014>;  
Jelescu et al. Neuroimage 2022: <https://doi.org/10.1016/j.neuroimage.2022.119277>;  
Callaghan et al. ArXiv preprint 2022: <https://arxiv.org/abs/2103.08237>.

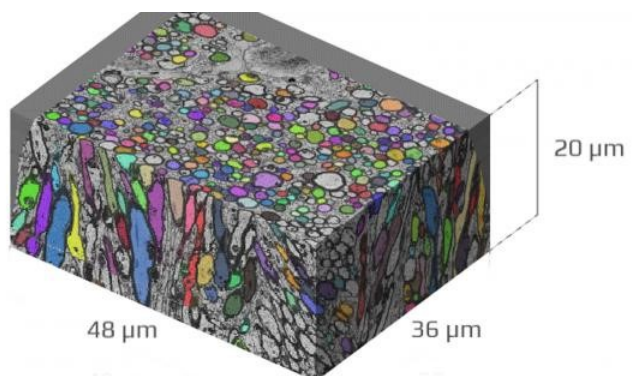
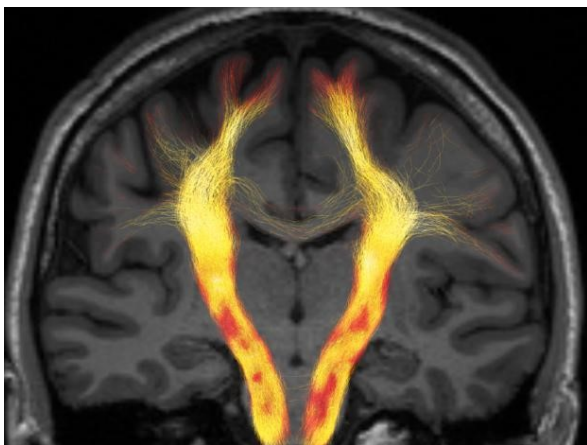
# Quantifying White Matter Microstructure using Diffusion MRI: validation and clinical translation

## Els Fieremans

NYU Langone, NY, US  
Department of Radiology

**Abstract:** Human MRI is limited to millimeter voxels, yet diseases develop at the cellular scale. In brain, microstructural content can be retrieved in vivo non-invasively using diffusion MRI. In this talk, we will explore novel strategies to glean microstructural information and disentangle between the different neurodegenerative processes underlying brain pathology. We will discuss the standard model used to describe the diffusion MRI signal in brain white matter, and the pitfalls in estimation of the standard models, including axonal water fraction, fiber dispersions, intra-, and extra-axonal diffusivities, and the free water fraction. At the same time, there is an urgent need for validation of the assumptions underlying biophysical models. These assumptions, along with the specificity of diffusion MRI to axonal features, are validated using realistic Monte Carlo simulations in 3-dimensional electron microscopy, and by comparison of diffusion MRI-derived features to their histological counterparts in animal models. Finally, we will demonstrate pathological specificity in various human clinical datasets of development and multiple pathologies.

**Bio:** Els Fieremans is Associate Professor and co-director of the MRI Biophysics group at the Center for Biomedical Imaging, Department of Radiology, New York University Grossman School of Medicine. She received her master's degree in physics and PhD in Biomedical Engineering from Ghent University, Belgium. The goal of her research is to leverage quantitative MRI towards specificity on the cellular scale, through biophysical modeling and validation using numerical and physical phantoms, in order to find the earliest and most sensitive markers of brain disease.



# Relaxation Anisotropy in Biological Tissues

Nina E. Hänninen<sup>1,2</sup>, Timo Liimatainen<sup>1,3</sup>, Matti Hanni<sup>1,3,4</sup>, Olli Gröhn<sup>5</sup>, Miika T. Nieminen<sup>1,3,4</sup>, Mikko J. Nissi<sup>1,2</sup>

<sup>1</sup> Research Unit of Medical Imaging, Physics and Technology, University of Oulu, <sup>2</sup> Department of Applied Physics, University of Eastern Finland, <sup>3</sup> Department of Diagnostic Radiology, Oulu University Hospital, <sup>4</sup> Medical Research Center, University of Oulu and Oulu University Hospital, <sup>5</sup> A.I. Virtanen Institute for Molecular Sciences, University of Eastern Finland

**Introduction:** Highly organized tissues, such as skeletal muscle<sup>1</sup>, tendon<sup>2,3</sup>, white matter<sup>4,5</sup> and cartilage<sup>6</sup>, are reported to exhibit varying relaxation times when MRI measurements are conducted at different physical orientations with respect to the main magnetic field<sup>7-9</sup>. Previously, orientation dependence of multiple relaxation parameters has been investigated in cartilage<sup>10</sup>. In this study, we expand the investigation of relaxation anisotropy to several tissue types, including tendon, myocardium, kidney, and brain tissue.

**Methods:** Four mice were sacrificed in compliance with ethical permits and were transcatheterially perfused and fixed with 4 % PFA. Heart, brain, kidney and a piece of spinal cord were collected and stored in 4 % PFA. Cartilage and tendon samples were collected from four bovine knees obtained from a local grocery store. A custom-built holder attached to an Arduino controlled device allowed automatic rotation of the samples inside the MRI scanner. MRI was performed at 9.4 T using a 19 mm quadrature RF volume transceiver and VnmrJ3.1 Varian/Agilent DirectDrive console. Relaxation time measurements were acquired using a global preparation block coupled to a single slice fast spin echo readout. All measurements were obtained at five different sample orientations with respect to the main magnetic field  $B_0$ , and they included: IR-T1, MESE T2, Adiabatic T1 $\rho$ , continuous wave (CW)-T1 $\rho$  (500 Hz) and RAFF2<sup>11</sup>. The images were co-registered to the first orientation using Elastix software<sup>12</sup> and pixel-wise relaxation time maps were calculated. Relaxation anisotropy was computed pixel-wise as Michelson contrast<sup>10</sup>:  $(R_i^{\max} - R_i^{\min}) / (R_i^{\max} + R_i^{\min})$ , where  $R_i$  is the relaxation rate ( $1/T_i$ ).

**Results and Conclusion:** The clearest anisotropic patterns were observed for T2, CW-T1 $\rho$  and RAFF2 in cartilage and tendon samples (Figure 1). T2 relaxation anisotropy in deep cartilage was 70% and in 30% tendon. Adiabatic T1 $\rho$  and T1 demonstrated very little anisotropy in tendon and cartilage. In the other tissue types, i.e. brain, spinal cord, myocardium and kidney relaxation anisotropy was generally 5% or lower for all the measured relaxation parameters. The results confirm that highly ordered collagenous tissues have properties that induce very clearly observable relaxation anisotropy, whereas in other tissues the effect is not as prominent. Quantitative comparison of anisotropy of different relaxation parameters highlights the importance of sequence choice and design in MR imaging.

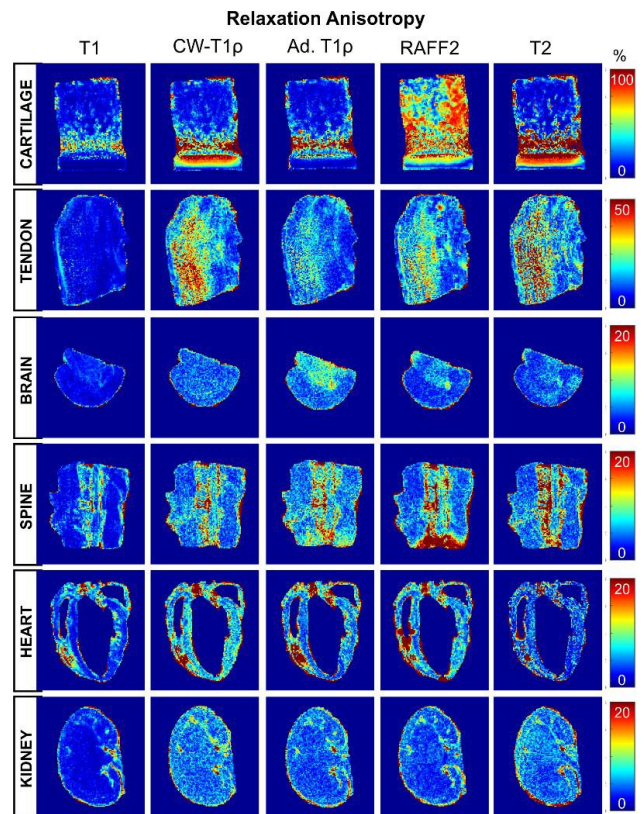


Figure 1. Relaxation anisotropy maps of multiple relaxation parameters in different tissue types.

<sup>1</sup> Cleveland, G. G. et al. Biophysical journal 16, 1043–53 (1976); <sup>2</sup> Fullerton, G. et al. Radiology 155, 433–435 (1985); <sup>3</sup> Navon, G. et al. Journal of Magnetic Resonance Imaging 25, 362–380 (2007); <sup>4</sup> Bender, B. et al. NMR in Biomedicine 23, 1071–1076 (2010); <sup>5</sup> Rudko, D. A. et al. Proc Natl Acad Sci U S A 111, E159–67 (2014); <sup>6</sup> Xia, Y. Magnetic Resonance in Medicine 39, 941–949 (1998); <sup>7</sup> Erickson, S. J. et al. Radiology 188, 23–25 (1993); <sup>8</sup> Lee, J. et al. Neuroimage 57, 225–234 (2011); <sup>9</sup> Nieminen, M. T. et al. in Biophysics and Biochemistry of Cartilage by NMR and MRI (eds. Xia, Y. & Momot, K. I.) 147–175 (Royal Society of Chemistry, 2017); <sup>10</sup> Hänninen, N. et al. Scientific Reports 7, 9606 (2017); <sup>11</sup> Liimatainen, T. et al. Magnetic Resonance in Medicine 64, 983–994 (2010); <sup>12</sup> Klein, S. et al. IEEE Transactions on Medical Imaging (2010)

# Automated segmentation of myelinated axons in multi-resolution 3D electron microscopy images

Ali Abdollahzadeh<sup>1</sup>, Andrea Behanova<sup>2</sup>, Ilya Belevich<sup>3</sup>, Eija Jokitalo<sup>3</sup>, Alejandra Sierra<sup>1</sup>, Jussi Tohka<sup>1</sup>

<sup>1</sup>A. I. Virtanen Institute for Molecular Sciences, University of Eastern Finland, Kuopio, Finland, <sup>2</sup>Department of Information Technology, Uppsala University, Uppsala, Sweden, <sup>3</sup>Electron Microscopy Unit, Institute of Biotechnology, University of Helsinki, Helsinki, Finland

Advances in electron microscopy (EM) have made it possible to image brain ultrastructures three-dimensional (3D) by employing serial-sectioning methods. We have developed a series of automated tools for segmentation and morphology analyses of myelinated axons imaged at high and low resolutions using 3D-EM techniques. These tools are automatic 3D segmentation of axons (ACSON) [1], deep convolutional neural networks (CNNs)-based ACSON (DeepACSON) [2], and graphical user interface (GUI) for ACSON (gACSON) [3]. The ACSON pipeline was developed based on a region-growing algorithm segmenting myelinated axons in small field-of-view high-resolution 3D-EM datasets. We developed DeepACSON to segment myelinated axons in large field-of-view low-resolution 3D-EM images automatically. DeepACSON performs CNN-based semantic segmentation and applies a novel cylindrical shape decomposition algorithm to exploit the tubularity of myelinated axons in the instance segmentation [4]. gACSON is an easy-to-use GUI for ACSON, allowing interactive segmentation, visualization, or correction of a segmented ultrastructural component. gACSON also applies instance segmentation of myelin, mapping myelin sheaths to their corresponding intra-axonal spaces, and adds myelin thickness and g-ratio to the set of measurable morphological parameters.

Using ACSON and gACSON, we segmented hundreds of myelinated axons in high-resolution datasets and with DeepACSON hundreds of thousands of long-span myelinated axons in low-resolution datasets. These tools could deal with the challenges of 3D-EM segmentation and achieve excellent evaluation scores in automated segmentation of myelinated axons, offering new ways to unravel the actual morphology of myelinated axons.

[1] Abdollahzadeh A, et al. *Sci. Rep.* 9(1):6084 (2019). [2] Abdollahzadeh A, et al. *DeepACSON Automated Segmentation of White Matter in 3D Electron Microscopy*. *Communications Biology* 4(1):179 (2021). [3] Behanova, A, et al. *Computer Methods and Programs in Biomedicine* 220, 106802 (2022). [4] Abdollahzadeh A, et al. *IEEE Access* 9: 23979–95 (2021).

# What Does FEXI Measure?

Mohammad Khateri<sup>1</sup>, Marco Reisert<sup>2</sup>, Alejandra Sierra<sup>1</sup>, Jussi Tohka<sup>1</sup>, and Valerij G. Kiselev<sup>2</sup>

<sup>1</sup>Ai Virtanen Institute for Molecular Sciences, University of Eastern Finland, <sup>2</sup>Medical Physics Department of Radiology, University Medical Center Freiburg, Faculty of Medicine, University of Freiburg, Freiburg, Germany

**Introduction:** Inspired by the diffusion exchange spectroscopy technique (DEXSY) [1, 2], the double pulsed-gradient spin echo (PGSE) sequence with stimulated echo was modified to have gradients pairs of different magnitude. This gave rise to the filter-exchange imaging (FEXI) [3] for measuring the apparent exchange rate (AXR) between compartments with different diffusivities. The first gradient pair acts as a mobility filter suppressing the signal from the compartment with high diffusivity. The second gradient pair measures the diffusion coefficient for different mixing times, revealing the recovery to the unperturbed value. The specific exchange mechanism is not crucial for the functioning of the method. The present revival of interest in such measurements is inspired by possible biomedical applications. In this context, FEXI is commonly considered as a way to access the cell membrane permeability for water.

In this work, we show that FEXI is not uniquely sensitive to the transcytolemmal exchange, but also to the geometry of involved compartments. In a complicated geometry, water in narrow spaces with limited mobility in the filter gradient direction can avoid suppression by the mobility filter and then move during the mixing time to less restricted locations where it contributes to a high diffusivity. This can occur without crossing any membrane. To illustrate this mechanism, we use Monte Carlo (MC) simulations in large compartments of simple to complex geometries with impermeable boundaries, shown in Fig. 1. While these substrates do not include any permeable membranes, our simulation results show several cases of spurious transcytolemmal exchange that can lead to misinterpretation of data.

**Methods:** We generated a set of three-dimensional media with variable geometrical complexity (Fig. 1a-c). For MC simulations, we used a C++ program, which was previously developed for simulating transverse relaxation, diffusion, and the Larmor frequency shift [4-7].

**Results:** The FEXI result for considered media are shown in Fig. 1 for diffusion inside tubes or spheres. The most pronounced spurious exchange is present for the most complex geometries. The magnitude of the effect and spurious exchange time decrease for simpler geometries.

**Discussion and conclusion:** Summarizing this study with an answer to the question in the title, FEXI does measure exchange, but exchange mediated by both the membrane permeation and diffusion within individual compartments of tortuous geometry.

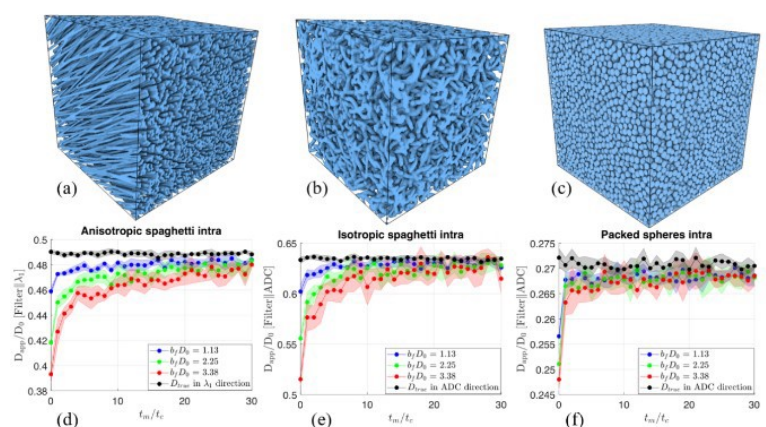


Figure 1: Simulation results for diffusion in intra-space of considered media, color bands at one standard deviation. Panels (d-f) show results for the coinciding directions of mobility filter and the measurement. A pronounced spurious exchange is seen for most complex geometries (Fig 1. (d) - (e)), while this exchange is insignificant for simplest geometries (Fig 1. (f)).

1. Callaghan PT, Furo I. The Journal of chemical physics. 2004 Feb 22;120(8):4032-8. 2. Marcel Gratz, et al. Microporous and mesoporous materials, 125(1-2):30-34, 2009. 3. Ingrid Aslund, et al. Journal of Magnetic Resonance, 200(2):291-295, 2009. 4. Dmitry S. Novikov, et al. Journal of Magnetic Resonance, 293:134 - 144, 2018. 5. Dmitry S. Novikov, et al. Journal of Magnetic Resonance, 195(1):33-39, November 2008. 6. Alexander Ruh, et al. Magnetic resonance in medicine, 79(2):1101-1110, Feb 2018. 7. Alexander Ruh, et al. Journal of Magnetic Resonance, 307:106584, 2019.

# Automatic cerebral hemisphere segmentation in rat MRI with lesions via attention-based convolutional neural networks

**Juan Miguel Valverde**

A. I. Virtanen Institute for Molecular Sciences, University of Eastern Finland, Kuopio, Finland

We present MedicDeepLabv3+, a convolutional neural network that is the first completely automatic method to segment cerebral hemispheres in magnetic resonance (MR) volumes of rats with lesions. MedicDeepLabv3+ improves the state-of-the-art DeepLabv3+ with an advanced decoder, incorporating spatial attention layers and additional skip connections that, as we show in our experiments, lead to more precise segmentations. MedicDeepLabv3+ requires no MR image preprocessing, such as bias-field correction or registration to a template, produces segmentations in less than a second, and its GPU memory requirements can be adjusted based on the available resources. We optimized MedicDeepLabv3+ and six other state-of-the-art convolutional neural networks (DeepLabv3+, UNet, HighRes3DNet, V-Net, VoxResNet, Demon) on a heterogeneous training set comprised by MR volumes from 11 cohorts acquired at different lesion stages. Then, we evaluated the trained models and two approaches specifically designed for rodent MRI skull stripping (RATS and RBET) on a large dataset of 655 MR rat brain volumes. In our experiments, MedicDeepLabv3+ outperformed the other methods, yielding an average Dice coefficient of 0.952 and 0.944 in the brain and contralateral hemisphere regions. Additionally, we show that despite limiting the GPU memory and the training data, our MedicDeepLabv3+ also provided satisfactory segmentations. In conclusion, our method, publicly available at <https://github.com/jmlipman/MedicDeepLabv3plus>, yielded excellent results in multiple scenarios, demonstrating its capability to reduce human workload in rat neuroimaging studies.

## **A multiscale tissue assessment in a rat model of mild traumatic brain injury**

**Isabel San Martín Molina**<sup>1</sup>, Michela Fratini<sup>2,3</sup>, Gaetano Campi<sup>4</sup>, Manfred Burghammer<sup>5</sup>, Tilmann Grunewald<sup>5</sup>, Raimo A. Salo<sup>1</sup>, Omar Narvaez<sup>1</sup>, Manisha Aggarwal<sup>6</sup>, Jussi Tohka<sup>1</sup>, and Alejandra Sierra<sup>1</sup>

<sup>1</sup>A.I. Virtanen Institute for Molecular Sciences, University of Eastern Finland, Kuopio, Finland; <sup>2</sup>Institute of Nanotechnology-CNR c/o Physics Department, Sapienza University of Rome, Italy; <sup>3</sup>IRCCS Fondazione Santa Lucia, Rome, Italy; <sup>4</sup>Institute of Crystallography, CNR, Rome, Italy; <sup>5</sup>European Synchrotron Radiation Facility, Grenoble Cedex, France; <sup>6</sup>Russell H. Morgan Department of Radiology and Radiological Science, John Hopkins University School of Medicine, Baltimore, United States

Mild traumatic brain injury (mTBI) is a major health problem worldwide, affecting approximately between 200-700 out of 100,000 people per year. Microstructural tissue changes associated with mTBI are usually not detectable by conventional magnetic resonance imaging (MRI) techniques. Thus, the aim of this study was to evaluate the potential and limitations of diffusion tensor imaging (DTI) to detect tissue microstructural changes after mTBI in combination with light microscopy and scanning micro-X-ray diffraction (S $\mu$ XRD) to characterize the tissue at multiple scales.

We induced mTBI in adult male Sprague-Dawley rats (mTBI n = 3; sham-operated n = 2) using the lateral fluid percussion injury ( $0.97 \pm 0.06$  atm). Thirty-five days after sham-operation or mTBI, ex vivo DTI was performed in a 11.7 T Bruker NMR spectrometer. After the scans, the brains were processed for histology, and sections were stained for Nissl and myelin (gold chloride staining) to assess cellularity and myelinated axons using automated cell counting and structure tensor-based analyses, respectively. S $\mu$ XRD was done at the ID13 beamline of the European Synchrotron Radiation Facility, and derived information of the myelin structure at the nanoscale level. We analyzed the ipsilateral corpus callosum, cingulum, external capsule, internal capsule and layer VI of the somatosensory cortex at - 2.00 mm from bregma. Furthermore, we constructed a multiple regression model to assess the relationship between these three imaging modalities.

Our findings revealed DTI changes, axonal damage, reduced myelin density and gliosis in histology, and different stages of ultrastructural degeneration of myelin in S $\mu$ XRD maps after mTBI. We found moderate correlations between DTI and histological techniques, and low correlation between S $\mu$ XRD to histology and DTI. Altogether, these results indicate the potential of DTI to moderately detect loss of myelinated axons and gliosis, and low detection of ongoing ultrastructural damage of the myelin. In summary, our multiscale imaging study opens new ways to examine mild tissue damage using multiple imaging modalities and their detection by non-invasive MRI methods.

# White matter characterization by massively multidimensional diffusion-correlation MRI

Omar Narvaez<sup>1</sup>, Leo Svenningsson<sup>2</sup>, Maxime Yon<sup>2</sup>, Daniel Topgaard<sup>2</sup>, and Alejandra Sierra<sup>1</sup>

<sup>1</sup>A.I. Virtanen Institute for Molecular Sciences, University of Eastern Finland, Kuopio, Finland, <sup>2</sup>Department of Chemistry, Lund University, Lund, Sweden

Massively multidimensional diffusion-correlation MRI uses free gradient waveforms to acquire images by modifying the trace ( $b$ ), normalized anisotropy ( $b_{\Delta}$ ), orientation ( $\theta, \phi$ ), centroid frequency ( $\omega_{cent}$ ) with variable repetition ( $\tau_R$ ) and echo time ( $\tau_E$ ) to obtain nonparametric  $D(\omega)$ - $R_1$ - $R_2$ -distributions<sup>[1]</sup>. Once the tensor distributions are obtained, an arbitrary set of “bins” limits are selected on the squared normalized anisotropy ( $D_{\Delta 2}$ ) and isotropic diffusivity ( $D_{iso}$ ) plane to visualize the tissue fractions (i.e., white matter and gray matter) and cerebrospinal fluid<sup>[2]</sup>. Each tissue has different diffusivity, anisotropy, and chemical properties; thus, it is important to characterize each fraction to understand the changes that might occur during pathologies.

To expand the tissue classification to not only in the  $D_{\Delta 2}$  and  $D_{iso}$  plane, we use the unsupervised k-means clustering method including the information of  $D_{\Delta 2}$ ,  $D_{iso}$ ,  $R_1$  and  $R_2$  to characterize the components of the white matter. We perfused intracardially 5 rats with 4% paraformaldehyde (PFA). Both optic nerves were removed from each brain and incubated in a solution of 4% PFA, 1% glutaraldehyde and gadolinium for scanning. Each scan consisted of 737 images using free gradient waveforms varying  $b$ ,  $b_{\Delta}$ , ( $\theta, \phi$ ),  $\omega_{cent}$ ,  $\tau_R$ , and  $\tau_E$ . The total scan time was  $\sim 20$  hours. The images were denoised and then, the inversion algorithm was applied to obtain the nonparametric distributions using the same parameters as previous studies<sup>[1]</sup>. The mean distributions  $E[D_{\Delta 2}]$ ,  $E[D_{iso}]$ ,  $E[R_1]$  and  $E[R_2]$  across the 10 optic nerves were plotted in a 3D scatter plot (Fig.1, a) with  $E[D_{\Delta 2}]$ ,  $E[D_{iso}]$  and  $E[R_1]$  on the axes and  $E[R_2]$  as the color-code. K-means clustering was applied with a  $k=3$ . The 3 clusters obtained in white matter are displayed in Fig.1, b; where it can be observed the contribution of each parameter to each cluster. These results shows that cluster 1 has the biggest contribution from  $E[D_{\Delta 2}]$ ,  $E[R_1]$  and  $E[R_2]$ ; cluster 2 shows a significant reduction of  $E[D_{\Delta 2}]$ , as well of  $E[R_1]$  and  $E[R_2]$ ; and cluster 3 has the smallest contribution of  $E[D_{\Delta 2}]$  with similar contribution of  $E[D_{iso}]$  as cluster 1

and 2 but with almost no contribution of  $E[R_1]$ . The cluster 1 is conformed by 88% percent of the data, cluster 2 by 9% and cluster 3 by 3%. Each cluster might be related to the different elements in white matter (e.g., myelinated axons, glial cells, capillaries).

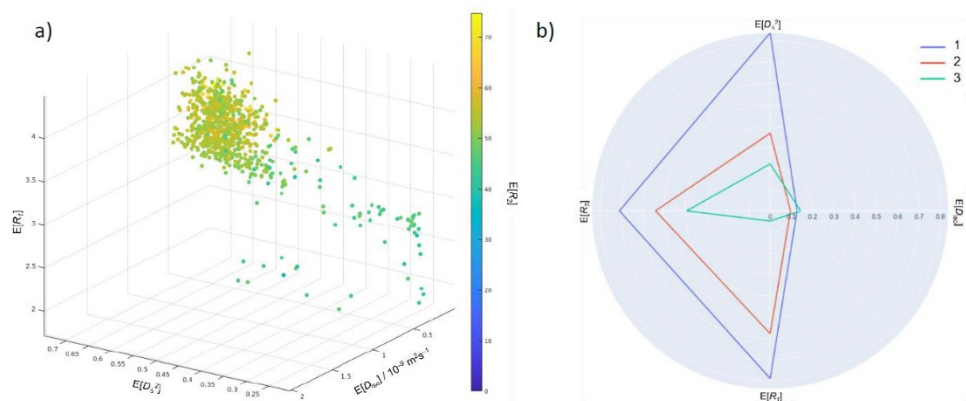


Figure 1. a) 3D Scatter plot of the mean distribution of  $E[D_{\Delta 2}]$ ,  $E[D_{iso}]$ ,  $E[R_1]$  from all the optic nerves. The color-code are the  $E[R_2]$  values. b) The clusters obtained are represented in a

Our results show the potential of massively multidimensional diffusion-relaxation correlation acquisitions to disentangle the per voxel microstructure information of white matter. Furthermore, the characterization of the clusters by diffusivities, anisotropy, and relaxation rates of white matter would allow a better understanding of the subtle changes during pathologies.

[1] Narvaez et al., 2022. doi: 10.3389/fphy.2021.793966 [2] Topgaard, 2019. doi:10.1002/nbm.4066

## **Apply multi-modal fMRI to study neuro-glio-vascular network function in different brain states**

### **Xin Yu**

Massachusetts General Hospital, Harvard University, MA, US  
Athinoula A. Martinos Center for Biomedical Imaging

In this talk, I will first introduce two novel fMRI imaging methods: line scanning and single-vessel fMRI. These methods map laminar- and vessel-specific fMRI responses with ultra-high spatial and temporal resolution using high field MRI in animals. The line-scanning mapping scheme enables the investigation of neuronal circuit-specific contribution to layer-specific BOLD signals in both evoked and resting states. The single-vessel fMRI allows us to specify the vascular hemodynamic responses from individual arterioles and venules. Both mapping schemes have been translated for human brain mapping. In the second part of this talk, I will introduce the multi-modal fMRI platform to combine fiber photometry with fMRI to specify unique gliovascular coupling events to distinct astrocytic Ca<sup>2+</sup> transients. By deciphering the neuro-glio-vascular interactions, we will better understand the brain-wide fMRI responses corresponding to different brain states.

## fMRI using a ZTE sequence

### Ian Shih

University of North Carolina, NC, US  
Department of Neurology

Gradient-recalled echo (GRE)-based echo planar imaging (EPI) has been the gold standard functional magnetic resonance imaging (fMRI) technique for nearly three decades due to its ability to rapidly acquire whole brain volumes with MR T2\* sensitivity to blood oxygenation — a well-known surrogate marker for brain activity. This immensely utilized technique, however, suffers from high acoustic noise, ghosting and motion artifacts, magnetic field inhomogeneity-related artifacts, low sensitivity compared to other neuroimaging modalities, and poor spatial specificity. An fMRI sampling technique that addresses these problems has the potential to change day-to-day fMRI practices. In particular, such a development would be of great benefit to the emerging rodent fMRI community as anesthesia, stress, and susceptibility artifact confounds can be avoided. Aptly, imaging sequences with “zero” acquisition delay and minimal increment of gradients are insensitive to problems stated above and have the potential to provide superior specificity and sensitivity compared to GRE-EPI-fMRI. To explore the utility of a hard-pulse-based zero-echo-time (ZTE) based sequence for fMRI, we modeled ZTE contrast mechanisms, modified its sequence design for fMRI, and examined parameters that may augment ZTE-fMRI sensitivity. We also implemented a PCB-based head-fixation coil which allows the use of ZTE-fMRI in awake mice. We hope the results brought by these efforts to have positive influences to fMRI methods with short acquisition delay, including ZTE and multi-band SWIFT.

# **In vivo direct imaging of neuronal activity at high temporo-spatial resolution**

## **Jang-Yeon Park**

Sungkyunkwan University (SKKU), South Korea

Department of Biomedical Engineering

There has been a longstanding demand for noninvasive neuroimaging methods capable of detecting neuronal activity at both high temporal and spatial resolution. In this talk, I will introduce a novel approach that enables Direct Imaging of Neuronal Activity (termed DIANA) for functional MRI that can dynamically image spiking activity in milliseconds precision, achieved by rapid k-space line scan synchronized with periodically applied functional stimuli. DIANA was demonstrated through in vivo mice brain imaging at 9.4 T during electrical whisker-pad stimulation. DIANA had high correlations with spike activities, which could be applied in capturing the sequential and laminar-specific propagation of neuronal activity along the thalamocortical pathway, as further confirmed through in vivo spike recording and optogenetics. In terms of contrast mechanism, DIANA was almost unaffected by hemodynamic responses, but was sensitive to changes in neuronal activity-associated tissue relaxation times such as T2 relaxation time. DIANA is expected to open up new avenues in brain science by providing a deeper understanding of the brain's functional organization including the temporo-spatial dynamics of neural networks.

# Whole-brain studies of spontaneous behavior in head-fixed rats enabled by zero echo time MB-SWIFT fMRI

Jaakko Paasonen<sup>a</sup>, Petteri Stenroos<sup>a</sup>, Hanne Laakso<sup>a</sup>, Tiina Pirttimäki<sup>a</sup>, Ekaterina Paasonen<sup>a</sup>, Raimo A. Salo<sup>a</sup>, Heikki Tanila<sup>a</sup>, Djaudat Idiyatullin<sup>b</sup>, Michael Garwood<sup>b</sup>, Shalom Michaeli<sup>b</sup>, Silvia Mangia<sup>b</sup>, Olli Gröhn<sup>b</sup>

<sup>a</sup> A. I. Virtanen Institute for Molecular Sciences, University of Eastern Finland, Kuopio, Finland; <sup>b</sup> Center for Magnetic Resonance Research, University of Minnesota, Minneapolis, USA

**Introduction:** Understanding the link between the (ab)normal brain activity and behavior, during, e.g., motivation, emotions, or decision-making, is a key challenge in modern neuroscience. Behavioral neuroscience, however, lacks tools to record whole-brain activity in complex behavioral settings. Here we demonstrate that a novel Multi-Band SWEEP Imaging with Fourier Transformation (MB-SWIFT) functional magnetic resonance imaging (fMRI) approach enables, for the first time, whole-brain studies in spontaneously behaving head-fixed rats. MB-SWIFT is a 3D radial zero echo time sequence with large bandwidths and minimal gradient steps, making it quiet and insensitive to movement and field inhomogeneities.

**Methods:** Adult male Sprague-Dawley rats ( $n = 10$ ) were used. An implant for head-fixation was attached (Fig. 1A). The rats were habituated to fMRI for 9 days. Rats wore a soft walking harness and ear plugs (Fig. 1B). During fMRI, the rat behavior was recorded with an MRI-compatible video camera (Fig. 1C). MRI was performed with Agilent 9.4 T magnet with a 21-cm bore and a custom-made transmit-receive loop coil (22 mm inner diameter). fMRI data (representative image in Fig. 1D) were acquired with a 3D MB-SWIFT (2000 spokes, TR 0.97 ms, temporal resolution  $\sim 2$  s, 192/384 kHz excitation/acquisition bandwidths,  $6^\circ$  flip angle, and 643 matrix size with  $625 \mu\text{m}$  isotropic resolution). Each rat underwent fMRI 1-3 times (15-25 min, 450-750 fMRI volumes each). Positioning to the holder and MRI adjustments were performed while the rats were under sevoflurane (2-3%) anesthesia. Data were processed and analyzed with in-house made scripts, Matlab, Python, ANTs, FreeSurfer, Aedes, and FSL.

**Results:** The group-level independent component analysis of the data obtained from head-fixed rats indicated anatomically relevant whole-brain functional parcellation (Fig 2A). Additionally, we detected sensory, motor (Fig 2B), exploration, and stress-related brain activity in relevant networks during corresponding spontaneous behavior observed in recorded video. Moreover, we measured odor-induced activation of olfactory system with high correlation between the fMRI and behavioral responses (Fig 2C).

**Conclusion:** We conclude that the applied methodology enables novel behavioral study designs in rodents focusing on tasks, cognition, emotions, physical exercise, and social interaction. Importantly, novel zero echo time and large bandwidth approaches, such as MB-SWIFT, can be applied for human behavioral studies, allowing more freedom as body movement is dramatically less restricting factor.

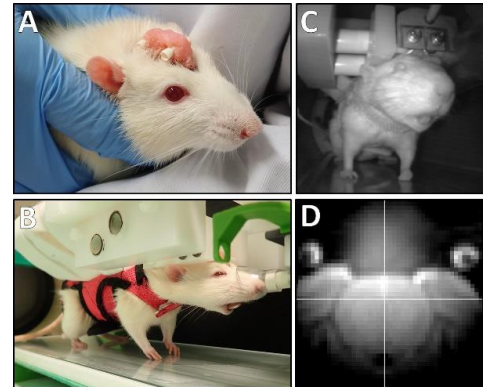


Figure 1. A head implant (A), a rat wearing a walking harness in the MRI holder (B), a rat inside the MRI scanner (C), and a representative MB-SWIFT fMRI image (D).

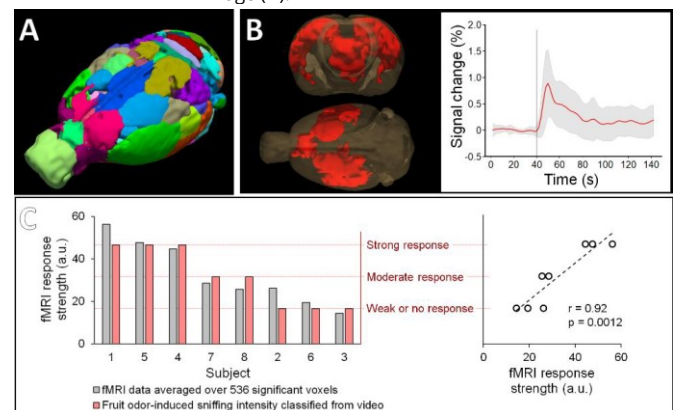


Figure 2. ICA-based functional parcellation (A), fMRI response during spontaneous motoric activity (B), and excellent correlation between behavioral and fMRI responses (C).

# Spinal cord fMRI with MB-SWIFT for assessing epidural spinal cord stimulation in rats

Hanne Laakso<sup>1,2</sup>, Lauri J Lehto<sup>1,2,3</sup>, Jaakko Paasonen<sup>1</sup>, Raimo Salo<sup>1</sup>, Antonietta Canna<sup>2,4</sup>, Igor Lavrov<sup>5,6,7</sup>, Shalom Michaeli<sup>2</sup>, Olli Gröhn<sup>1</sup>, Silvia Mangia<sup>2</sup>

<sup>1</sup> A.I. Virtanen Institute for Molecular Sciences, University of Eastern Finland, Kuopio, Finland <sup>2</sup> Center for Magnetic Resonance in Research, University of Minnesota, Minneapolis, MN, United States <sup>3</sup> Radiology, Kanta-Häme Central Hospital, Hämeenlinna, Finland <sup>4</sup> Department of Medicine, Surgery and Dentistry, "Scuola Medica Salernitana", Salerno, Italy <sup>5</sup> Kazan Federal University, Kazan, Russia <sup>6</sup> Department of Neurology, Mayo Clinic, Rochester, MN, USA <sup>7</sup> Department of Physiology and Biomedical Engineering, Mayo Clinic, Rochester, MN, USA

Electrical epidural spinal cord stimulation (SCS) is used as a treatment for chronic pain and holds potential for recovery after a spinal cord injury. Monitoring the spinal cord activity during SCS with functional MRI (fMRI) could provide important and objective measures of responses to treatment. Unfortunately, spinal cord fMRI is severely challenged by motion and susceptibility artefacts induced by the implanted electrode and bones. This study introduces Multi-Band SWEEP Imaging with Fourier Transformation (MB-SWIFT) technique for spinal cord fMRI during SCS in rats. Given the close to zero acquisition delay and high bandwidth in three dimensions, MB-SWIFT is highly tolerant to motion and susceptibility induced artefacts, and thus holds promise for spinal cord fMRI during SCS.

Here, MB-SWIFT with 3-s temporal resolution was used at 9.4T in rats undergoing epidural SCS at different frequencies. Its performance was compared with spin echo EPI and the origin of the functional contrast was also explored using suppression bands. MB-SWIFT was found to be tolerant to electrode-induced artefacts and to respiratory motion, leading to substantially higher fMRI sensitivity than with spin echo EPI (Fig 1A). We demonstrated that MB-SWIFT allows robust detection of fMRI responses in the spinal cord, even in the presence of electrodes (Fig 1B). Clear stimulation frequency dependent responses to SCS were detected in the rat spinal cord close to the stimulation site (Fig 1B,C). The origin of MB-SWIFT fMRI signals was found consistent with dominant inflow effects.

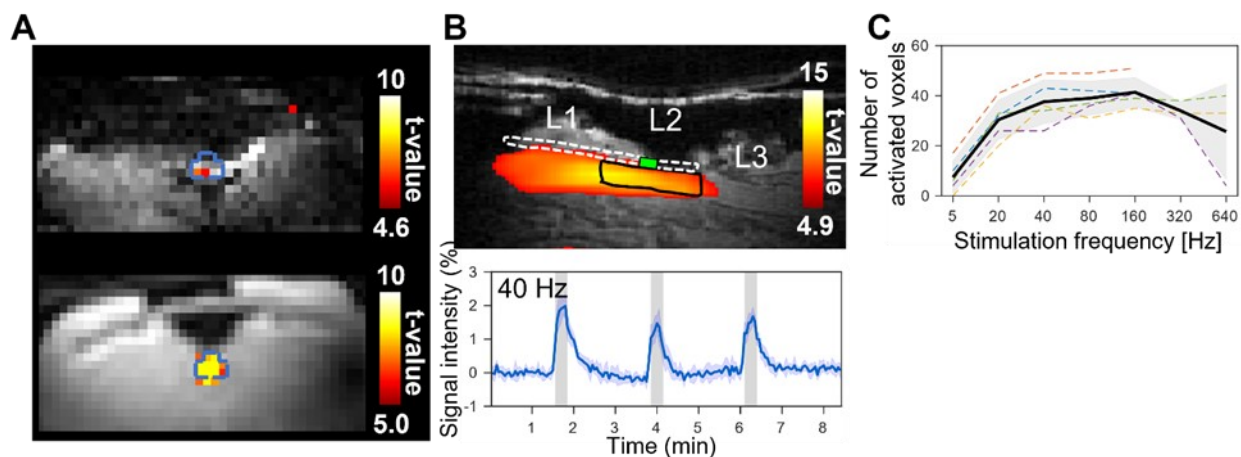


Figure 1. Comparison between spin echo EPI and MB-SWIFT fMRI of the spinal cord during spinal cord stimulation (A), response to stimulation at the frequency of 40 Hz under the stimulation site in spinal cord (B), and dependence of fMRI signals detected with MB-SWIFT on the stimulation frequency shown by the mean number of activated voxels within the L2 region.

In conclusion, fMRI of the rat spinal cord during SCS can be reliably achieved using MB-SWIFT, thus providing a valuable experimental framework for assessing the effects of SCS on the central nervous system.

## Light sedation with short habituation time for large-scale fMRI studies in rats

Lenka Dvořáková<sup>1</sup>, Petteri Stenroos<sup>1,2</sup>, Ekaterina Paasonen<sup>1</sup>, Raimo A. Salo<sup>1</sup>, Jaakko Paasonen<sup>1</sup>, Olli Gröhn<sup>1\*</sup>

<sup>1</sup> A.I.V. Institute for Molecular Sciences, University of Eastern Finland, Kuopio, Finland, <sup>2</sup> Institute of Neuroscience, Grenoble, France

Traditionally, preclinical resting state functional magnetic resonance imaging (fMRI) studies have been performed in anesthetized animals. Nevertheless, as anesthesia affects the functional connectivity (FC) in the brain, there has been a growing interest in imaging in the awake state. Obviously, awake imaging requires resource- and time-consuming habituation prior to data acquisition to reduce the stress and motion of the animals. Light sedation has been a less widely exploited alternative for awake imaging, requiring shorter habituation times while still reducing the effect of anesthesia. To show, that light sedation is a valid alternative to the awake imaging, we measured 102 rats using the light sedation protocol and compared the outcomes with both onsite- and offsite- measured awake data.

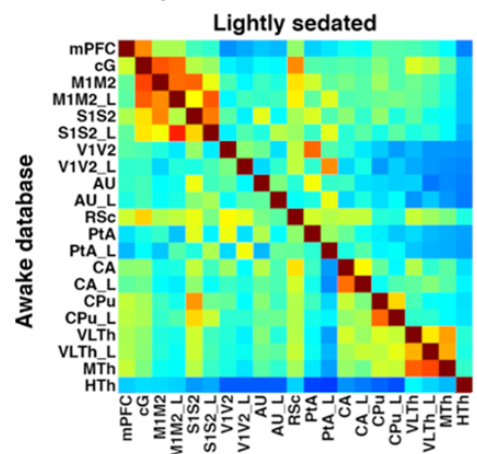
In this project, male Sprague Dawley rats were habituated and measured either under a light anesthesia (N = 102) or in an awake state (N = 10) as described before<sup>1</sup>. The habituation time was gradually increased from 15 to 35 minutes for the lightly sedated and up to 45 minutes for the awake animals for 3 days in the lightly sedated or 4 days for the awake animals. On the acquisition day, the fMRI was measured for 25 minutes.

Even with habituating protocol, the animal still tends to occasionally move during the acquisition. Hence, an automated preprocessing pipeline of the fMRI data was developed on-site to accommodate datasets affected by motion. In addition to the traditional preprocessing pipeline (slice timing correction, motion correction, and registration to a reference brain), we have implemented a motion scrubbing and independent component analysis (ICA) based approach for motion removal. In motion scrubbing, frames with the biggest motion are discarded from the data based on their framewise displacement<sup>2</sup>. The ICA analysis was performed for each subject and the non-neuronal components were automatically regressed out of the data. The same pipeline was also applied to the open dataset of resting-state fMRI in awake rats, which consists of 289 measurements in 90 rats<sup>2</sup>.

For the functional connectivity analyses a set of 21 regions of interest (ROIs) were drawn on the reference brain according to the anatomical atlas. A sliding window was used to determine the motion-free parts of the signal and the correlation coefficient was then calculated as the mean value from the windows.

The functional connectivity (FC) pattern in the lightly sedated group is very similar to both awake groups. The mean FC matrices of the lightly sedated and the open awake database are shown in the figure on the right. The correlation values in the cortico-cortical regions are slightly higher in the lightly sedated group and on the other hand, the correlation values in the subcortical and cortico-subcortical showed a slight decrease in the lightly sedated group. Nevertheless, the correlation between the two correlation matrices was high. Moreover, less data were excluded due to motion with the light sedation than had been needed with the open awake rat database while the light sedation demands shorter habituation times.

We have shown that light sedation after a short habituation protocol can provide a good alternative approach for large-scale fMRI studies.



<sup>1</sup>Dvořáková L et al. (2021). NMR in Biomedicine, e4679. <sup>2</sup>Liu Y et al. (2020). NeuroImage, 220, 117094.

# Event-recurring multiband SWIFT functional MRI with 200-ms temporal resolution in rat

E. Paasonen<sup>1,2</sup>, J. Paasonen<sup>1</sup>, L.J. Lehto<sup>2</sup>, T. Pirttimäki<sup>1,3</sup>, H. Laakso<sup>1</sup>, L. Wu<sup>2</sup>, J. Ma<sup>2</sup>, D. Idiyatullin<sup>2</sup>, H. Tanila<sup>1</sup>, S. Mangia<sup>2</sup>, S. Michaeli<sup>2</sup>, O. Gröhn<sup>1</sup>

<sup>1</sup> A. I. Virtanen Institute for Molecular Sciences, University of Eastern Finland, Kuopio, Finland, <sup>2</sup> Center for Magnetic Resonance Research, University of Minnesota, Minneapolis, MN, USA, <sup>3</sup> Department of Psychology, University of Jyväskylä, Jyväskylä, Finland

The purpose of this study was to develop a high temporal resolution functional MRI method for tracking repeating events in the brain. Our novel method uses using multiband sweep imaging with Fourier transformation (SWIFT) and is called event-recurring SWIFT (EVER-SWIFT). The resampling approach relies on the recognition that similar repeating events can be tracked with higher temporal resolution than a single event by combining data from several events. (Fig. 1A), achieving subsecond resolution. Here, we demonstrate the use of EVER-SWIFT for detecting functional MRI responses during deep brain stimulation of the medial septal nucleus and during spontaneous isoflurane-induced burst suppression in the rat brain at 9.4 T with 200-ms temporal resolution.

The EVER-SWIFT approach showed that the shapes and time-to-peak values of the response curves to deep brain stimulation significantly differed between downstream brain regions connected to the medial septal nucleus, resembling findings obtained with traditional 2-second temporal resolution. In contrast, EVER-SWIFT allowed for detailed temporal measurement of a spontaneous isoflurane-induced bursting activity pattern, which was not achieved with traditional temporal resolution (Fig. 1B).

The EVER-SWIFT technique enables subsecond 3D imaging of both stimulated and spontaneously recurring brain activities, and thus holds great potential for studying the mechanisms of neuromodulation and spontaneous brain activity.

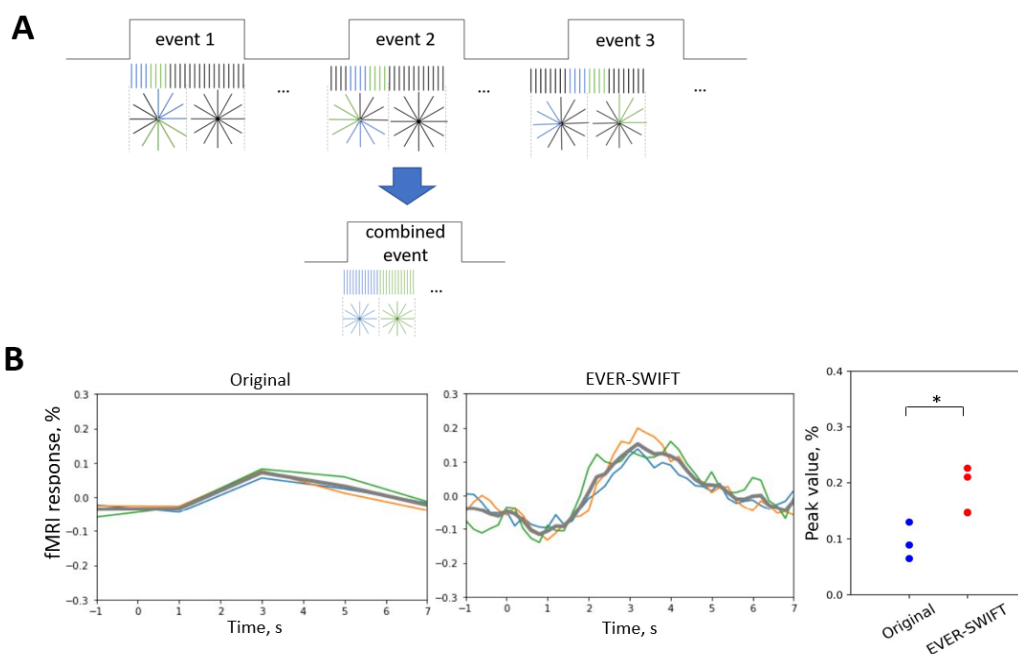


Figure 1. A. Resampling scheme for similar events. B. Comparison between 2-s temporal resolution and EVER-SWIFT in showing activation during isoflurane burst suppression pattern.

# Isoflurane affects brain functional connectivity in rats 1 month after exposure

Petteri Stenroos

A. I. Virtanen Institute for Molecular Sciences, University of Eastern Finland, Kuopio, Finland

Isoflurane, the most common preclinical anesthetic, causes brain plasticity and long-term molecular and cellular changes which can lead to behavioral and cognitive alterations. These changes are most likely associated with network-level changes in brain function. However, no studies have been conducted to evaluate the long-term effects of isoflurane on brain function at whole-brain level. In this study, we investigated the influence of a single isoflurane exposure on functional connectivity, brain electrical activity, and gene expression.

Male Wistar rats ( $n = 22$ ) were exposed to 1.8% isoflurane for 3 hours. Control rats ( $n = 22$ ) spent 3 h in the same environment without exposure to isoflurane. After 1-month from the treatment, functional connectivity was evaluated with resting-state functional magnetic resonance imaging (fMRI;  $n = 6 + 6$ ) and local field potential (LFP) measurements ( $n = 6 + 6$ ) in anesthetized animals. A whole genome expression analysis ( $n = 10+10$ ) was conducted with mRNA-sequencing from cortical and hippocampal tissue samples.

MRI-results showed that isoflurane treatment increased thalamo-cortical and hippocampal-cortical correlation (Figure 1). Also, cortical fMRI power was significantly increased in response to the isoflurane treatment. Local field potential results demonstrated strengthened hippocampal-cortical alpha and beta coherence, being in good agreement with the fMRI findings. Altered gene expression was found in 20 cortical genes, many of which are involved in neuronal signal transmission. However, no gene expression changes were found in the hippocampus.

Isoflurane induced long-term changes in thalamo-cortical and hippocampal-cortical function and expression of cortical genes involved in signal transmission in the cortex. Further studies are required to investigate whether these functional changes are associated with the postoperative behavioral and cognitive alterations commonly observed in patients and animals. Also, a potential for using isoflurane, as a neuroplasticity enhancer, for therapeutic purposes in managing neurocognitive disorders needs further assessments.

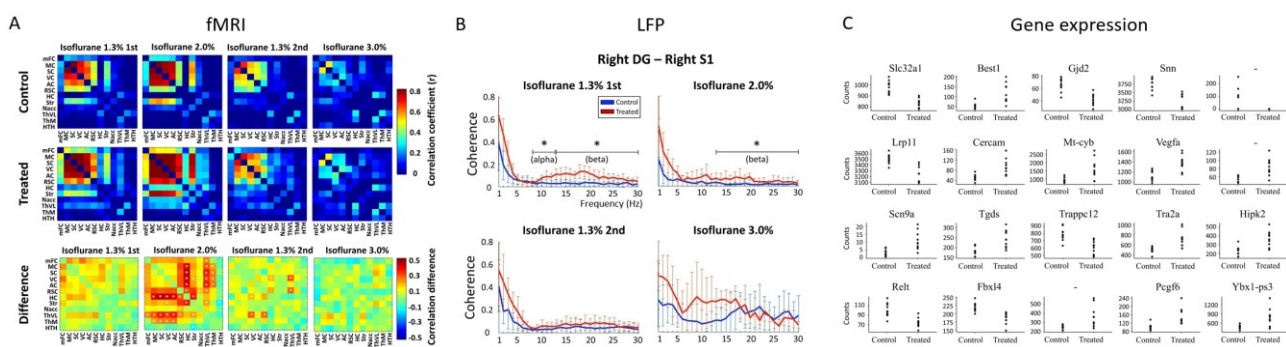


Figure 1. fMRI (A), LFP (B) and gene expression (C) changes 1 month after a single 3h 1.8% isoflurane treatment. MRI and LFP were measured under 1.3, 2.0 or 3.0% isoflurane concentrations. Thalamo-cortical and hippocampal-cortical connectivity (A) and hippocampal-cortical coherence (B) was significantly increased in response to treatment. Also, gene expression in cortex was significantly changed in 20 genes involved in signal transmission (C). DG = dentate gyrus, S1 = primary somatosensory cortex.

# Quantitative MRI biomarkers of post-traumatic epilepsy and cognitive impairment after lateral fluid-percussion injury

Eppu Manninen<sup>(1)</sup>, Karthik Chary<sup>(1)</sup>, Riccardo De Feo<sup>(1)</sup>, Elina Hämäläinen<sup>(1)</sup>, Niina Lapinlampi<sup>(1)</sup>, Pedro Andrade<sup>(1)</sup>, Tomi Paananen<sup>(1)</sup>, Alejandra Sierra<sup>(1)</sup>, Jussi Tohka<sup>(1)</sup>, Olli Gröhn<sup>(1)</sup>, and Asla Pitkänen<sup>(1)</sup>

<sup>(1)</sup> A.I. Virtanen Institute for Molecular Sciences, University of Eastern Finland

**Objective:** Currently, no treatments exist for post-traumatic epileptogenesis. Trials of antiepileptogenic treatments are expensive because there is no effective screening to select patients that are likely to develop epilepsy. We studied the injured cortex, the thalamus, and the hippocampus after lateral fluid-percussion-induced traumatic brain injury (TBI) to predict the development of post-traumatic epilepsy.

**Methods:**  $T_2$ ,  $T_2^*$ , and diffusion tensor imaging (DTI) parameter maps were acquired for rats in the preclinical EPITARGET MRI cohort using a 7-Tesla scanner on day (D) 2, D7, and D21 after TBI or sham-operation. Animals with post-traumatic epilepsy were determined from 1-month-long video-EEGs starting at 6 months post-TBI. Cognitive impairment was tested using Morris water maze on D35-39.

In the cortical analysis, total volumes of different classes of  $T_2$  abnormalities were determined and used in logistic regression models to predict (1) lesion progression, and (2) the development of post-traumatic epilepsy.

In the thalamic analysis,  $T_2$  and DTI parameters in the ventral posterior nucleus were determined and used in regularized logistic regression models to predict the development of post-traumatic epilepsy.

In the hippocampal analysis,  $T_2$ ,  $T_2^*$ , and DTI parameters along the hippocampal septotemporal axis were determined and used to model (1) the development of post-traumatic epilepsy, (2) cognitive impairment.

**Results:** Lesion size measurement on D7 predicted subsequent lesion size on D21 ( $p < 0.001$ , cross-validated  $R^2 = 0.83$ ). However, the progression of lesion size did not predict the development of post-traumatic epilepsy ( $p = 0.43$ ).

Regularized logistic regression of D7 and D21 MRI parameters in the ventral posterior thalamic nucleus predicted the development of post-traumatic epilepsy with a cross-validated area under the receiver operating characteristic curve (ROC AUC) of 0.78 (95% confidence interval 0.66-0.86).

Regularized logistic regression of MRI measures in the contralateral hippocampus at 3.4 mm from the temporal end predicted cognitive impairment (ROC AUC 0.72, 95% confidence interval 0.55-0.84). Hippocampal MRI did not predict the development of post-traumatic epilepsy.

**Significance:** Early cortical MRI presents a prediction of lesion size growth. This information could be used to select animals with the greatest need of neuroprotection for trials of neuroprotective treatments.

Thalamic MRI presents a prediction for the development of post-traumatic epilepsy. This information could be used to select animals most likely to develop post-traumatic epilepsy for trials of antiepileptogenic treatments.

Hippocampal MRI presents a prediction of cognitive impairment. This information could be used to pinpoint the hippocampal pathologies that can cause cognitive impairment.

# Simultaneous, preclinical PET/ MRI: Is it worth the investment?

## Uwe Himmelreich

University of Leuven, Belgium

Biomedical MRI, Department Imaging and Pathology

Multi-modal imaging is becoming more and more popular in order to overcome limitations in sensitivity, specificity or resolution of individual imaging techniques. Undoubtedly, this has resulted in an increase of information, cross-validation and also quantification of in vivo imaging experiments. However, it also requires increased investments in imaging infrastructure and frequently in lengthier imaging studies. Therefore, it is important to carefully assess when multi-modal imaging is indeed necessary to answer research and clinical questions.

Multi-modal imaging can be acquired either on separate scanners, on imaging scanners that operate in-line but acquire images sequentially or on scanners that integrate multiple imaging techniques for simultaneous data acquisition. Simultaneous data acquisition on integrated systems is faster but also more demanding in terms of the design of the instrument.

During this presentation, an overview of simultaneous vs. sequential acquisition PET/ MRI approaches and applications for preclinical imaging will be provided. Applications will be explained where simultaneous acquisition is not really needed, where it is a nice add on and where simultaneous acquisition is necessary to answer specific research questions.

### Review articles:

Bailey DL et al. Combined PET/MRI: Global Warming—Summary Report of the 6th International Workshop on PET/MRI. *Mol Imaging Biol* (2018) 20:4-20.

Wehrl HF et al. Combined PET/MR Imaging – Technology and Applications. *Technol. Cancer Res. Treat.* (2010) 9: 5-20

Pyatigorskaya N et al. Contribution of PET-MRI in brain diseases in clinical practice. *Curr Opin Neurol* (2020) 33: 430-438

Manabe O et al. Positron emission tomography/MRI for cardiac diseases assessment. *Brit J Radiol* (2020) 93: 20190836

Beyer T et al. What scans we will read: imaging instrumentation trends in clinical oncology. *Cancer Imag* (2020) 20:38.

## What can hyperpolarized $^{13}\text{C}$ MRS tell us about kidney disease?

### Christoffer Laustsen

Aarhus University, Denmark

MR research centre

Kidney disease is a growing serious condition with diabetes being the largest risk factor for developing end stage kidney disease (ESKD).

In order to arrest or even reverse the kidney complications seen in diabetes patients. A greater biological insight into the devastating changes the kidneys experience during prolonged hyperglycemia. This calls for better diagnostic methods for the earlier identification of patients at risk of developing kidney diseases. Accurately determining what treatment individual patients should receive and how the patient responds to treatment is of even greater importance. In this talk I will introduce you to some of the key findings we have obtained over the years in this area and discuss what this technology can tell us about kidney disease.

# Switching electron spins ON and OFF. D-DNP using non-persistent radicals: from photo-chemistry to hyperpolarization storage

## Andrea Capozzi

École Polytechnique Fédérale de Lausanne, Switzerland  
Institute of Physics

Technical University of Denmark, Denmark  
Department of Electrical Engineering

Since its invention in 2003, dissolution Dynamic Nuclear Polarization (d-DNP) has become the most powerful and versatile method to enhance Nuclear Magnetic Resonance (NMR) sensitivity in the liquid state. Without a doubt, the most important success is the unique opportunity to perform Magnetic Resonance Imaging (MRI) for staging of cancer and early treatment monitoring by means of injection of metabolically relevant hyperpolarized substrates.

Despite its undisputed potential, hyperpolarization via dDNP struggles to enter the clinic on a daily base because the method relies on expensive and technically demanding hardware: the so-called d-DNP polarizer.

The technique builds on a method known since the 50s' under the name of simply DNP: if sufficiently low temperature (1 - 4 K) and high magnetic field (3.5 - 7 T) are provided, microwave irradiation at the right frequency can enhance the substrate NMR signal in the solid state by transferring polarization from few unpaired electron spins (e.g. organic free radicals) duly added to the sample.

Unfortunately, the same electron spins, in absence of microwave irradiation, represent the main source of NMR signal loss. When extracting the sample from the polarizer, the only way to shelter its hyperpolarization is to create enough distance between the substrate and the unpaired electrons, hence the dissolution step. But, once in the liquid-state, the lifetime of the hyperpolarized substrate is limited to few tens of seconds. As a consequence, each MR facility willing to perform hyperpolarized studies has to be equipped with a d-DNP polarizer on-site.

From some years, I am working on making hyperpolarization transportable. In this talk I will describe one possible approach based on labile radicals.

# Simultaneous fMRI and metabolic MRS of hyperpolarized [1-<sup>13</sup>C]pyruvate during nicotine stimulus in rat

Viivi Hyppönen<sup>1</sup>, Jessica Rosa<sup>1</sup>, Mikko Kettunen<sup>1</sup>

<sup>1</sup>Kuopio Biomedical Imaging Unit, A.I. Virtanen Institute for Molecular Sciences, University of Eastern Finland, Kuopio, Finland

**Introduction:** Nicotine is often used as a stimulant in fMRI as it increases local cerebral glucose utilization on its binding sites<sup>1</sup>. It induces strong BOLD effect at cortical regions of the brain under urethane anesthesia and also increases CBF and CBV, giving strongest response 1-2 minutes after injection<sup>2</sup>. BOLD effect is also dose dependent<sup>3</sup>. Hyperpolarized carbon, so far mainly [1-<sup>13</sup>C]pyruvate, can be also used to study real-time cerebral metabolism. However, pre-clinically used anesthesia has also an effect on the apparent brain metabolism of hyperpolarized [1-<sup>13</sup>C]pyruvate possibly via cerebral circulation<sup>4,5</sup>. Here, we performed simultaneous <sup>1</sup>H fMRI and metabolic <sup>13</sup>C MRS during nicotine stimulus to compare their response.

**Methods:** Rats (n=11) were urethane anesthetized and their physiology was monitored during the experiment. [1-<sup>13</sup>C]pyruvic acid was hyperpolarized, dissolved with Tris buffer, neutralized with NaOH and injected (0.8 mmol/kg) to an animal inside the magnet. During experiment, each animal received two injections of pyruvate (with about 3 h apart) preceded by either nicotine or saline control injection 60 seconds before hyperpolarized [1-<sup>13</sup>C]pyruvate injection. The order of nicotine and saline injections was varied between animals. MRI data were collected at 9.4 T using a <sup>1</sup>H/<sup>13</sup>C transmit/receive surface coil and Agilent console. Pulse sequence collected fMRI data followed by one slice-selective <sup>13</sup>C MRS spectra with one cycle taking 2 s. We analyzed cortical, subcortical and muscle regions for fMRI. For <sup>13</sup>C, the first 90 seconds following pyruvate injection were summed and peak integrals calculated.

**Results:** In pilot experiments, simultaneous fMRI and <sup>13</sup>C MRS did not lead to degradation of signal compared to individual experiments. Proton signal from cortex increased 12% ± 4% (p<0.01) following nicotine injection, whereas no subcortical nor intramuscular signal change was observed. Saline injection did not change the observed signal. No change in lactate labelling was observed between saline and nicotine experiments, but an increase in bicarbonate-to-total-carbon ratio (p~0.03) and a trend towards increased bicarbonate-to-lactate (p~0.06) ratios were seen in four out of six rats after nicotine injection.

**Discussion & conclusions:** Simultaneous fMRI and <sup>13</sup>C MRS experiments were feasible in preclinical setting. This complementary information may allow a better assessment of the brain response to stimulus. While a clear cortical fMRI response was observed, MRS responses were more modest. An increase in bicarbonate levels was observed but there was no change in lactate labelling. Unlike in fMRI, only a very narrow time window can be observed with <sup>13</sup>C MRS. In the current study, timing between nicotine and pyruvate injections was chosen based on biggest changes on previously reported BOLD responses<sup>2</sup>, which were similar to the ones seen in the current study. However, brain activation following nicotine injection can change individually and local CBV peaks have been reported even over 10 minutes after nicotine injection<sup>6</sup>. It is therefore possible that the timing of experiment was not optimal and some other drug or model would lead to stronger responses on metabolic side as well. Alternatively, hyperpolarized glucose might reveal metabolic response more clearly<sup>7</sup>.

<sup>1</sup> London et al. J Neurosci. 1988, <sup>2</sup> Paasonen et al. Eur Neuropsychopharmacol. 2016, <sup>3</sup> Brujinzeel et al. Int J Neuropsychopharmacol. 2014, <sup>4</sup> Josan et al. Magn Reson Med. 2013, <sup>5</sup> Hyppönen et al. NMR Biomed. 2021, <sup>6</sup> Choi et al. Synapse. 2006, <sup>7</sup> Mishkovsky et al. Sci Reports 2021